Surface & Coatings Technology 253 (2014) 161–165

Contents lists available at ScienceDirect

Surface & Coatings Technology

journal homepage: www.elsevier.com/locate/surfcoat

Pulsed laser deposition of carbon nanodot arrays using porous alumina membranes as a mask

S.A. Hevia [a,b,*], P. Homm [a], F. Guzmán [c], H.M. Ruiz [a], G. Muñoz [a], L.S. Caballero [a], M. Favre [a,b], M. Flores [c]

[a] Instituto de Física, Pontificia Universidad Católica de Chile, Av. Vicuña Mackenna, 4860 Santiago, Chile
[b] Centro de Investigación en Nanotecnología y Materiales Avanzados "CIEN-UC", Av. Vicuña Mackenna, 4860 Santiago, Chile
[c] Departamento de Física, Facultad de Ciencias Físicas y Matemáticas, Universidad de Chile, Av. Blanco Encalada, 2008 Santiago, Chile

ARTICLE INFO

Article history:
Received 6 February 2014
Accepted in revised form 15 May 2014
Available online 24 May 2014

Keywords:
Carbon nanodots
Porous alumina
Pulsed laser deposition

ABSTRACT

Carbon nanodot arrays (CNA) are grown on silicon substrates by using pulsed laser deposition and porous alumina membranes as a mask. The masks are grown directly on silicon substrates, thus allowing the fabrication of homogenous CNAs on macroscopic areas. Reproducible CNAs were grown using an argon background in the deposition chamber, at pressures up to 17 mTorr. Carbon plasma plumes were analysed to examine the properties of the ejected materials and surface analysis techniques were employed to characterize the resulting CNAs.

1. Introduction

The possibility of growing regular nanodot arrays (NA) of different materials is an attractive topic due to their potential application in different fields, such as optoelectronic devices, information storage, sensors and microscopy [1–6]. In particular, carbon nanodot arrays (CNA) have been used as a substrate for direct immobilization of DNA [7], electron field emitters [8], bioimaging devices [9], radiometric fluorescent nanosensors [10], and temperature probes [11], or to perform chemical analysis [12] and cytotoxicity studies [13], among others. Several techniques have been used to produce NA of different characteristics, which include a combination of cathodic arc plasma and anodic alumina pore arrays [14], hydrothermal processes [15], electrochemical synthesis [16], and template assisted pulsed laser deposition [17–19]. In order to broaden the applicability of NA it is necessary to explore their fabrication in extended areas with a high degree of reproducibility and low cost. In this work we report the fabrication of CNA with a method that meets these conditions. Extended CNAs on silicon substrates have been grown by using pulsed laser deposition (PLD) and porous alumina membranes (PAM) as a mask. The masks are grown directly on silicon substrates, which has comparative advantages over similar methods reported in the literature [14,17,20], improving reproducibility and allowing the fabrication of homogenous CNAs on macroscopic areas. Depending on the synthesis conditions, resulting CNAs can have a sp^3 bond content of up to 50%.

2. Experimental details

To produce the PAMs, high purity aluminium (99.999%) was deposited on polished n-type Si(100) wafers (1 to 10 Ω cm) by using electron beam evaporation. An evaporation rate of 0.2 nm/s was used and the vacuum chamber pressure was kept below 2×10^{-6} Torr throughout the evaporation process. The resulting aluminium film, with 5 μm thickness, was anodized at 40 V using a 0.3 M oxalic acid solution as electrolyte, which was cooled at 5 °C. In order to obtain a porous pattern with high regularity, and to have control on the final thickness of porous mask, we performed the anodization in two steps [21], as shown in Fig. 1. The anodization time of the first step should be calibrated according to the initial thickness of aluminium, aiming to leave a suitable aluminium thickness for the second anodization. For an initial aluminium thickness of 5 μm, the anodization time of the first step (under previously mentioned conditions) should be around 90 min. In order to selectively remove the first porous alumina layer we used a solution with 6.0 wt.% phosphoric acid and 1.8 wt.% chromic acid, kept at 60 ºC for 15 min. The second step of anodization was run under the same conditions as of the first step, yielding homogeneous and highly ordered PAMs with a final thickness between 250 and 500 nm. Before carbon deposition, an etching step is required in order to remove the alumina barrier layer at the bottom of the pores. This etching was carried out for 60 min by using a 5 wt.% phosphoric acid solution at room temperature. With this treatment the pores are widened without affecting the order of the membranes. Growing the PAM directly onto the silicon substrate avoids relying on Van der Waals force for proper bonding [8], which in turn requires high surface cleaning and precludes using thinner PAMs.

The PLD was carried out in a vacuum chamber (base pressure below 3×10^{-5} Torr) with an external laser source. We used a short, high

* Corresponding author at: Instituto de Física, Pontificia Universidad Católica de Chile, Av. Vicuña Mackenna, 4860; Santiago, Chile.
E-mail address: samuel.hevia@fis.puc.cl (S.A. Hevia).

http://dx.doi.org/10.1016/j.surfcoat.2014.05.031
0257-8972/

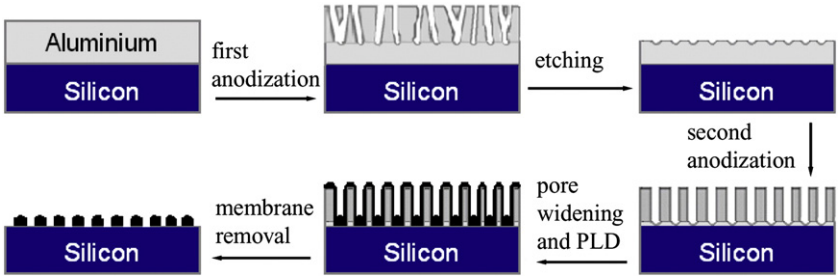

Fig. 1. Sch. of the CNA fabrication process. An aluminium layer is deposited on top of a silicon substrate, and then, by a double anodization process, the mask is fabricated. The widening of the pores is performed before the PLD. After deposition, the mask is removed with an etching treatment.

energy Nd:YAG laser pulse, 345 mJ, 4.4 ns, at 1.06 μm, focused onto a graphite target, at 7 J/cm^2 fluence. A porous alumina thin film attached to a silicon substrate was placed parallel to the target and located at 50 mm from the laser focal spot, in order to obtain a homogeneous deposit covering about one centimetre square. The growth rate was estimated close to 1 nm/s, from the ratio between thickness and deposition time of a carbon film on a silicon substrate. The exposure time ranged from 10 s to 120 s, with the laser operating at 10 Hz. Argon was also introduced in the vacuum chamber, in a pressure range from 8 to 170 mTorr, to investigate the effect of dominant carbon plasma species on the properties of the resulting nanodots. To remove the PAM mask with the carbon deposit, we used a 10 wt.% NaOH solution at room temperature between 15 min to 1 h, depending on the deposition condition.

The carbon films and nanodot arrays were characterized by several techniques. Scanning electron microscopy (SEM) was used to imagine the surface and a topographic study was carried out with atomic force microscopy (AFM). Raman micro-analysis, using a LabRam010 Spectrometer with a 632.8 nm laser excitation was performed in order to determine the binding state of carbon atoms in the samples.

Plasma characterization was carried out by optical emission spectroscopy (OES), in order to determine the carbon plasma species. The spectra were obtained with a Spectra Pro 275 (1200 g/mm) spectrometer, with a gated avalanche diode array, with 20 ms exposure time, and averaged over fifteen shots. A fast response, negative biased, Faraday cup was also used to measure the characteristic energy and flux of the plasma ions depositing onto the PAM.

3. Results and discussion

It has been found in previous investigations that a low pressure neutral background gas has a strong effect on plasma species composition of laser produced carbon plasma plumes [22]. To explore this effect on CNA growth, we introduced argon in the deposition chamber, at pressures ranging from 8 to 170 mTorr. We found that reproducible CNAs were obtained at base pressures, 8 mTorr and 17 mTorr. In all these cases, CNAs showed similar morphological properties, as inferred from SEM and AFM images. As the argon background pressure was increased up to 43 mTorr and beyond, we did not observe any nanodot formation. As we discuss below, this observation can be explained on the base of the observed plasma properties.

Fig. 2 shows SEM and AFM images of PAM used as a template and a characteristic CNA resulting from processes. Fig. 2(a) is a SEM top view image of the membrane with a histogram of the mean pore diameter, as obtained from the micrograph. Image 2(b) is a SEM top view of a CNA deposited at base pressure, with 10 s deposition time. We observe that both, regularity and shape of the porous are transferred to the nanodot arrays. Fig. 2(c) and (d) shows AFM topographic images of a PAM and CNA deposited at 8 mTorr, with 40 s deposition time, respectively. The distribution of porous and nanodots are consistent with the SEM images. In the PAM images, seen in Fig. 2(c) we observe a regular pattern of pores surrounded by "mounds" of alumina [23]. In this study, the average pore diameter of PAM was fixed to a value close to 66 nm (see histogram in Fig. 2a). This dimension, which is practically the dot diameter (obtained from the SEM image), can be tuned by changing the anodization parameters and the chemical etching time [5].

The thickness of the PAM mask is a critical parameter to be considered in NA fabrication. If the aspect ratio of the pore (height/diameter) is too large, the bottom of the pores becomes inaccessible to the materials containing the plasma plume. On the other hand, the PAM must be thick enough to ensure a good lift-off after deposition. As we have already mentioned, PAM without carbon deposited can be removed by using a solution with 6.0 wt.% phosphoric acid and 1.8 wt.% chromic acid at 60 °C per 15 min. This chemical etching is also suitable to carry out the lift-off of the mask when metals such as Au, Cu, Ag, Fe or Ni are deposited [5], but due the particular properties of the carbon films deposited in this case [24], its use was not effective. Alternatively, we used a 10 wt.% NaOH solution at room temperature between 15 min to 1 h, depending of deposit conditions. Employing sodium hydroxide is appropriate for this case; however, their use with others materials, as some transition metals, is not advisable. We found that PAM with thickness between 250 and 500 nm are suitable to fabricate these CNA; however, the shadow effect produced by the carbon deposited on the top and also in the pore wall might limit the height of the CN, as ballistic access to the pores bottom by carbon ions and molecules becomes impeded, leading to pore occlusion.

The main properties of amorphous carbon films are derived from the hybridization state of their carbon bonds. Of particular interest is the case of the diamond-like carbon (DLC) films, in which atoms are bonded mainly in sp^3 hybridizations. Micro-Raman spectroscopy was performed in order to determine the sp^3 contained in the CNA. Fig. 3 shows representative Raman spectra of CNA and carbon film before PAM removal, obtained at 8 mTorr argon pressure, with 40 s deposition time. Spectrum labelled R1 corresponds to the carbon deposit on top of the PAM, before using the treatment for mask removal. Spectrum labelled R2 corresponds to the CNA, resulting after PAM removal. Spectrum R1 can be fitted and deconvoluted in two main resonances, the D (1390 cm^{-1}) and G (1528 cm^{-1}) peaks, with a Lorentzian and a Breit–Wigner–Fano (BWF) function, respectively [25–27]. By using the tree-stage-model proposed by Ferrari [26], the percentage of sp^3 bonds content in the carbon deposit can be estimated around 20%, considering the peak positions and their intensity ratio (I(D)/I(G) ≈ 0.36); see Figs. 11 and 16 from reference [26]. As for the spectrum R2, it shows a characteristic resonance from the silicon substrate located between 900 and 1000 cm^{-1}, and a wide low intensity resonance around 1500 cm^{-1}. By amplifying the intensity of this peak by a factor of ten, we observe that this resonance exhibits a similar shape as in R1; however, these curves can be fitted using only the Breit–Wigner–Fano (BWF) function (1505 cm^{-1}). In this case, and using the same model as above, the sp^3 content in the nanodots is estimated to be around 50%. The reason of this higher content of sp^3 bonds, as compared with the deposit on the PAM, is due to the fact that the grow mechanism of carbon films on silicon is different from the one on the membrane. Further evidence that supports the estimation of sp^3 content in the nanodots is inferred

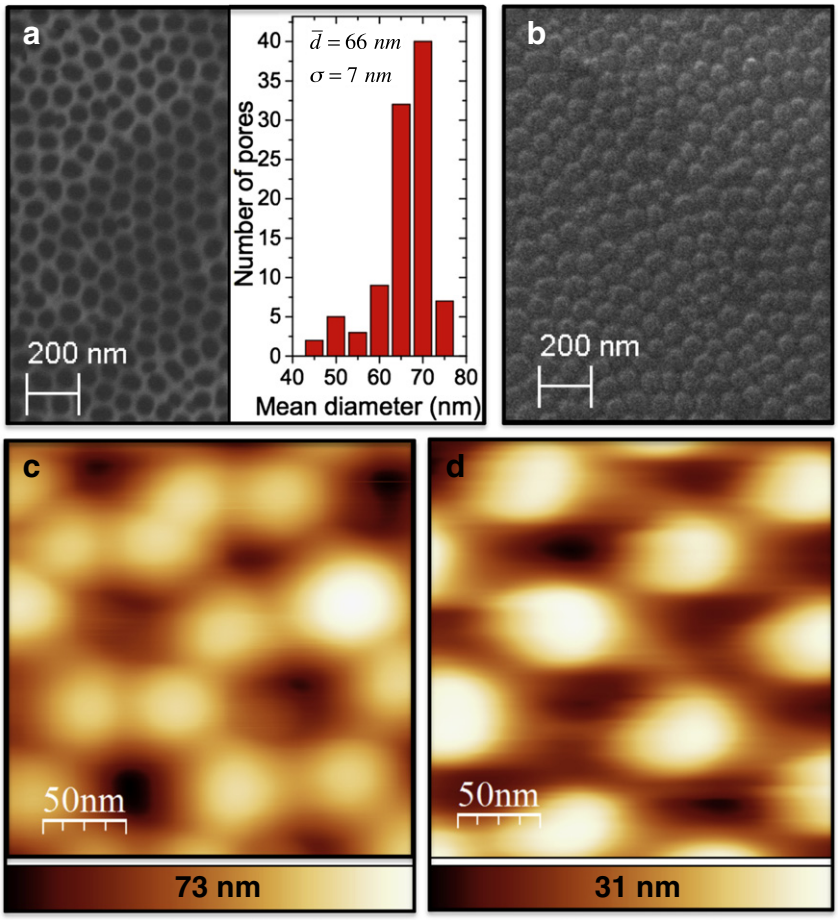

Fig. 2. Images (a) and (b) are top view SEM micrographs of PAM grown on top of a silicon substrate and resulting CNA, respectively. A histogram of the PAM pore diameter distribution is included on image (a). (c) and (d) correspond to AFM images of PAM used as a mask and the resulting CNA.

from previous experiments on the PLD of carbon films onto silicon substrates, using identical experimental conditions [32]. In that case an estimation of sp^3 content between 50 and 60%, for argon pressures up to a few tens of mTorr, as determined from Raman observations and using the tree-stage-model, was confirmed by an independent XPS characterization.

In order to correlate reproducible carbon nanodot growth with argon background pressure, we investigated the plasma plume by using OES and Faraday cup measurement. Simultaneous to the spectroscopy, performed just in the front region of the substrate, a deposit on a thicker PAM (20 μm) was carried out. Fig. 4 shows the spectrum of the carbon plasma emission collected from a point on an axis, located 50 mm from the target surface and the front of the substrate. The figure shows plasma emission at base pressure and with argon background in the range from 8 to 340 mTorr. With argon background the spectra are dominated by emission corresponding to vibrational states of the $d_3\Pi_g \rightarrow a^3\Pi_u$ Swan band, of the neutral C_2 molecule [28]. At base pressure the overall plasma emission is orders of magnitude below that with argon background, being the most prominent feature emission from C^+ ions. At higher pressures, where nanodot growth is not observed, the emission intensity increases significantly. A point to note is that the characteristic C_2 molecular density close to the PAM surface is higher than that observed at the same position in a free expanding laser plasma plume, at the same pressure. This is inferred from Fig. 5, where the integrated emission above continuum of the most prominent C_2 emission bands, $\Delta\nu = 1$ and $\Delta\nu = 0$, collected during the deposition process, from a point close to the PAM surface, and in the free expanding plasma, is plotted against argon pressure. In both cases C_2 emission is seen to reach a maximum around 80 mTorr, and then to decrease. This behaviour can be explained in terms of C_2 molecules' increased scattering as background pressure increases, and also a quenching effect on molecule formation due to carbon ions collisions with argon atoms. The fact that a higher C_2 density is observed next to the PAM, as compared to the free expanding laser plasma, is consistent with time resolved plasma images observations reported elsewhere [29], which show plasma stagnation at the deposition substrate surface for time scales up to a few microseconds.

Fig. 6 shows Faraday cup measurements, at different background pressures, obtained on an axis, at 50 mm from the graphite target, using a 1.7 cm^2 collecting area. This distance coincides with that where the PAM is located for CNA deposition. As the Faraday cup is negative biased, it also acts as an X-ray diode (XRD), being sensitive to extreme ultraviolet and soft x-ray (XUV) radiation [30]. As a consequence, the sharp spike at around $t = 0$ corresponds to XUV emission from the initial laser produced plasma. This can be used as a time mark to perform time of flight (TOF) measurements to determine the carbon ion energy spectra. The labels on the figure indicate characteristic energies for single ionized carbon atoms. The total ion dose collected by the Faraday cup remains constant around 3.4×10^{12} ions/cm^2, from base pressure up to near 100 mTorr, and decreases sharply up to one order of magnitude at around 160 mTorr.

The main issues that can be inferred from spectroscopic and Faraday cup measurements are a marked increase in C_2 molecule content in the laser plasma, as optical emission is proportional to molecular density, and a decrease in the characteristic energy of the carbon ions in the expanding plasma, both as argon background pressure increases. The trend in increasing C_2 molecule content in the expanding carbon plasma and decreasing characteristic carbon ion energy becomes more evident as the argon background pressure is further increased [30]. This

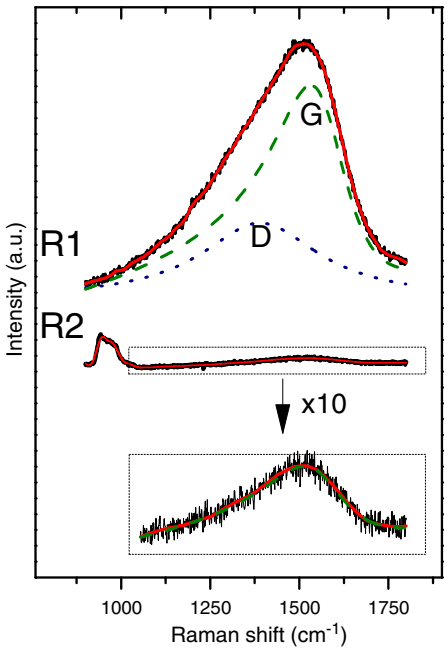

Fig. 3. Micro-Raman spectra: R1 corresponds to the carbon film deposited on top of the PAM, before the treatment used for mask removal. R2 corresponds to the CNA obtained at 8 mTorr argon pressure, with 40 s deposition time. Spectrum R1 is fitted and deconvoluted in two main resonances, the D and G peaks, with a Lorentzian and a Breit–Wigner–Fano (BWF) function, respectively [26]. By amplifying the intensity of the spectrum R2 by a factor of ten, a similar shape as in R1 is observed. The sp^3 content in these nanodots is estimated to be close to 50%.

enhancement in C_2 molecule formation has been explained previously in terms of a third-body effect, due to the presence of argon atoms, which favours C_2 formation by recombination of carbon atoms in the laser plasma plume [31]. It has also been observed that the expanding laser plasma is composed of several plasma fronts, being C^+ ions the main species in the first one, with C_2 molecules becoming dominant in the subsequent fronts [32]. The fact that no reliable carbon nanodot growth is observed at pressures above 17 mTorr might be linked to the laser plasma properties. As for the plasma composition, it can be argued that as the plasma content becomes dominated by C_2 molecules the deposition rate increases, up to a point that alumina pores become quickly blocked, thus precluding carbon ions entering and depositing inside the pores. A similar behaviour has been reported in DLC nanodot arrays growth using a combination of PAM and filtered cathodic arc plasma [8]. In this case no DLC nanodot arrays were obtained when

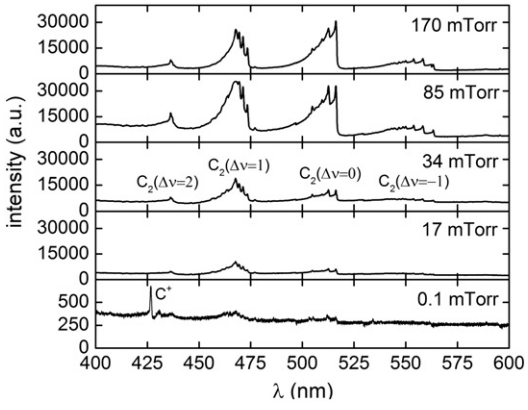

Fig. 4. Carbon plasma emission, at different argon background pressures, collected from a ~3 mm region located on the plasma plume axis, 50 mm from the graphite target surface. With argon background emission from the $d_3\Pi_g \rightarrow a^3\Pi_u$ Swan band of C_2 molecules is dominant.

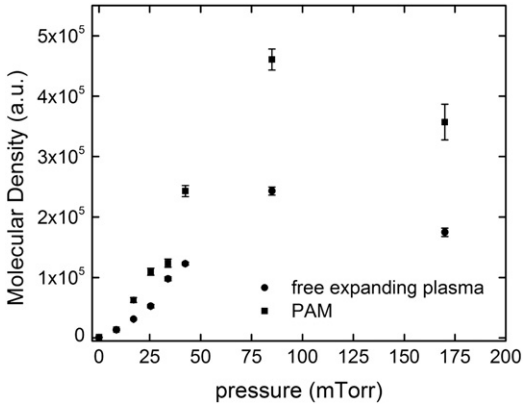

Fig. 5. Relative C_2 molecular density, as inferred from the integrated emission above continuum of the most prominent C_2 emission bands, $\Delta\nu = 1$ and $\Delta\nu = 0$. The spectroscopy was collected during the deposition process, from a point close to the PAM surface, and at the same position for the free expanding plasma.

the substrate bias was 0 V, whereas at −50 V bias, highly reproducible DLC nanodots arrays were obtained, thus indicating that a high deposition energy is required for the plasma ions to be deposited inside the porous. It has also been reported that when a laser produced carbon plasma expands in a low pressure argon background, carbon cluster formation is favoured, due to background gas ionization induced by charge transfer collisions with fast carbon ions [32–34]. It is then expected that as the characteristic cluster size increases, it becomes less likely for them to enter and deposit inside the alumina pores. Additionally, a decrease in the carbon ions characteristic energy results in a reduction of the mean free path for collisions, which in turns increases scattering and radial expansion of the expanding plasma. This is clearly linked to an increase in the argon background pressure. At lower pressures the carbon ions are more ballistic, due to larger mean free bath, so their chances to enter inside the pores are expected to be higher.

4. Conclusions

We have shown the feasibility of growing CNAs on a silicon substrate by depositing a laser produced carbon plasma over a porous alumina membrane grown directly on silicon substrates. Depending on the synthesis conditions, resulting CNAs have a sp^3 bond content of up to 50%. In this study the CN diameter was fixed close to 70 nm, but this dimension can be tuned by changing the synthesis parameters or the etching time. In a particular configuration of PLD parameters, the deposition time determined the high of the nanodots. The shadow effect produced by the carbon deposited on the membrane limited the height of the CN.

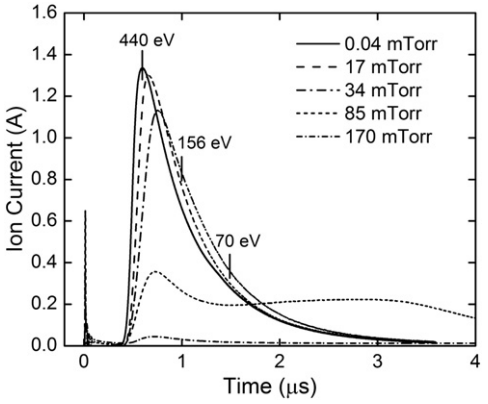

Fig. 6. Faraday cup signals collected on an axis, at 50 mm from the graphite target, at different argon background pressures. The labels indicate characteristic values of the energy associated with single ionized carbon atoms.

The presence of a low pressure argon background favours reliable CNA growth. However, as the argon background pressure increases, further nanodot growth is not observed. This is attributed to enhanced C_2 molecule and carbon cluster formation, resulting from the interaction of the expanding laser carbon plasma and the neutral gas background.

Conflict of interest

No conflict of interest.

Acknowledgement

This work has been funded by projects FONDECYT Nos. 11110352 and 1110380, and CONICYT PIA No. ACT1108. P. Homm and F. Guzmán acknowledge master and doctoral studies scholarships from CONICYT, respectively.

References

[1] S.P.A. Fodor, J.L. Read, M.C. Pirrung, L. Stryer, A.T. Lu, D. Solas, Science 251 (1991) 767–773.
[2] D.J. Lockhart, E.A. Winzeler, Nature 405 (2000) 827–836.
[3] C.K. Harnett, K.M. Satyalakshmi, H.G. Craighead, Appl. Phys. Lett. 76 (2000) 2466–2468.
[4] M. Kokonou, A.G. Nassiopoulou, K.P. Giannakopoulos, A. Travlos, T. Stoica, S. Kennou, Nanotechnology 17 (2006) 2146–2151.
[5] C.P. Li, I.V. Roshchin, X. Batlle, M. Viret, F. Ott, I.K. Schuller, J. Appl. Phys. 100 (2006) 074318-1-074318-7.
[6] M. Jung, W.A. El-Said, J.W. Choi, Nanotechnology 22 (2011) 235304–235308.
[7] T. Djenizian, E. Balaur, P. Schmuki, Nanotechnology 17 (2006) 2004–2007.
[8] S.C. Li, P.X. Yan, X.C. Li, E.M. Chong, Phys. E. 42 (2010) 1343–1346.
[9] B. Chen, F. Li, S. Li, W. Weng, H. Guo, T. Guo, X. Zhang, Y. Chen, T. Huang, X. Hong, S. You, Y. Lin, K. Zeng, S. Chen, Nanoscale 5 (2013) 1967–1971.
[10] S. Qu, H. Chen, X. Zheng, J. Cao, X. Liu, Nanoscale 5 (2013) 5514–5518.
[11] P.C. Chen, Y.N. Chen, P.C. Hsu, C.C. Shih, H.T. Chang, Chem. Commun. 49 (2013) 1639–1641.
[12] S. Chen, H. Zheng, J. Wang, J. Hou, Q. He, H. Liu, C. Xiong, X. Kong, Z. Nie, Anal. Chem. 85 (2013) 6646–6652.
[13] X. Zhang, X. He, Y. Li Xiao, Z. Zhang, Y. Ma, F. Li, J. Liu, J. Nanosci. Nanotechnol. 13 (2013) 5254–5259.
[14] P.J. Zhang, J.T. Chen, R.F. Zhuo, L. Xua, Q.H. Lu, X. Ji, P.X. Yan, Z.G. Wu, Appl. Surf. Sci. 255 (2009) 4456–4460.
[15] P.C. Hsu, H.T. Chang, Chem. Commun. 48 (2012) 3984–3986.
[16] H. Ming, Z. Ma, Y. Liu, K. Pan, H. Yu, F. Wang, Z. Kang, Dalton Trans. 41 (2012) 9526–9531.
[17] C.H. Bae, S.M. Park, S.C. Park, J.S. Ha, Nanotechnology 17 (2006) 381–384.
[18] X. Gao, L. Liu, B. Birajdar, M. Ziese, W. Lee, M. Alexe, D. Hesse, Adv. Funct. Mater. 19 (2009) 3450–3455.
[19] M. Gupta, V. Sauer, Y.Y. Tsui, Appl. Phys. A Mater. Sci. Process. 110 (2013) 817–821.
[20] W. Nam, H. Seo, S.C. Park, C.H. Bae, S.H. Nam, S.M. Park, J.S. Ha, Jpn. J. Appl. Phys. 43 (2004) 7793–7797.
[21] S. Hevia, P. Homm, A. Cortes, V. Núñez, C. Contreras, J. Vera, R. Segura, Nanoscale Res. Lett. 7 (2012) 342–348.
[22] H.M. Ruiz, F. Guzmán, M. Favre, H. Bhuyan, H. Chuaqui, Plasma Sources Sci. Technol. 21 (2012) 034014–034016.
[23] T. Xu, G. Zangari, R.M. Metzger, Nano Lett. 2 (2002) 37–41.
[24] J. Robertson, Mater. Sci. Eng. R (2002) 129–281.
[25] A.C. Ferrari, J. Robertson, Phys. Rev. B 61 (2000) 14095–14107.
[26] A.C. Ferrari, J. Robertson, Phys. Rev. B 64 (2001) 075414-1-075414-13.
[27] A.C. Ferrari, J. Robertson, Phil. Trans. R. Soc. A 362 (2004) 2477–2512.
[28] A. Kushwaha, R.K. Thareja, Appl. Opt. 47 (2008) G65.
[29] M. Favre, L.S. Caballero, H.M. Ruiz, F. Guzmán, H. Bhuyan, F. Veloso, E.S. Wyndham, Proc. 31st ICPIG, July 14-19, 2013, Granada, Spain, 2013.
[30] S.R. Mohanty, H. Bhuyan, N.K. Neog, R.K. Rout, E. Hotta, Jpn. J. Appl. Phys. 44 (2005) 5199–5205.
[31] S.M. Park, H. Chae, S. Wee, I. Lee, J. Chem. Phys. 109 (1998) 928.
[32] F. Guzmán, M. Favre, H.M. Ruiz, S. Hevia, L.S. Caballero, E.S. Wyndham, H. Bhuyan, M. Flores, S. Mändl, J. Phys. D. Appl. Phys. 46 (2013) 215202–215206.
[33] A. Bailini, P.M. Ossi, Appl. Surf. Sci. 252 (2006) 4364–4367.
[34] A. Bailini, P.M. Ossi, A. Rivolta, Appl. Surf. Sci. 253 (2007) 7682–7685.